

# On Samples of Satellite Measurement Data for Constructing a Global Model of the Magnetic Field of Mars

A. M. Salnikov<sup>\*,\*\*,a</sup>, A. V. Batov<sup>\*,\*\*,b</sup>, I. E. Stepanova<sup>\*\*,c</sup>, and T. V. Gudkova<sup>\*\*,d</sup>

<sup>\*</sup>Trapeznikov Institute of Control Sciences, Russian Academy of Sciences, Moscow, Russia

<sup>\*\*</sup>Schmidt Institute of Physics of the Earth, Russian Academy of Sciences,

Moscow, Russia

e-mail: <sup>a</sup>salnikov@ipu.ru, <sup>b</sup>batov@ipu.ru, <sup>c</sup>tet@ifz.ru, <sup>d</sup>gudkova@ifz.ru

Received June 5, 2024

Revised July 22, 2024

Accepted July 25, 2024

**Abstract**—In this work, we explore the challenges associated with the formation of satellite measurement datasets for constructing models of Mars’ magnetic field. Several approaches to dataset construction have been proposed and implemented. Using the regional method of S-approximations, analytical approximations of the magnetic field have been developed, and analytical continuations of the field to a uniform selected altitude have been presented. Calculations were performed for an area of Mars that includes the landing sites of the InSight spacecraft and the Chinese rover Zhurong. The modeling was based on datasets derived from calibrated insitu.calibrated level 2 data of the MAVEN mission.

*Keywords:* Mars, magnetic field, data samples, analytical continuation, S-approximation method

**DOI:** 10.31857/S0005117924100095

## 1. INTRODUCTION

Creating magnetometers for satellite measurements to measure the magnetic field of a planet is a highly complex task [1]. The first spacecraft to obtain magnetic field measurements of Mars were the Mariner 4 (flew by at a distance of 9850 km), “Mars-3” (closest approach  $\sim 1500$  km), “Mars-2”, “Phobos”, and “Phobos-2” (see review [2]). The authors of [2] believe that in early 1972 (approximately 25 years before MGS), “Mars-3” detected the magnetic field of the Martian crust.

Before the launch of Mars Global Surveyor (MGS) in 1996, little was known about Mars’ magnetic field, and its origin was debated. Previous missions only provided upper estimates of the planet’s magnetic moment intensity [3].

The hypothesis that Mars does not have a global magnetic field was confirmed by the MGS mission. The MGS spacecraft operated in Mars orbit from 1997 to 2006 and became the first mission to provide magnetic field measurements at sufficiently low altitudes to reveal the unique characteristics of the Martian magnetic field. Since September 1997, vector magnetic field observations have been obtained from more than 1000 elliptical orbits with closest approaches between 85 and 170 km [4].

A fairly strong magnetization was discovered in the southern hemisphere of the planet. Many maps and models of the planet’s magnetic field have been constructed based on MGS data [3, 5–11].

Thanks to the Mars Atmosphere and Volatile Evolution (MAVEN) mission, which has been operating in Mars orbit since the fall of 2014, we have new data that has been combined with MGS

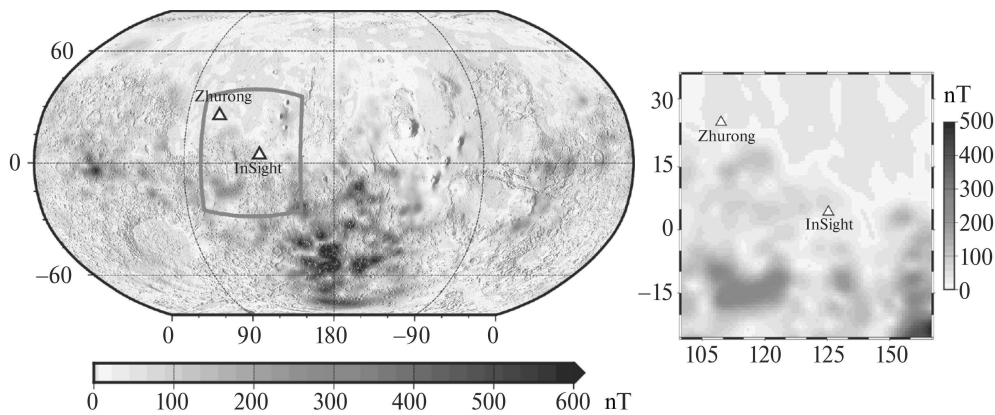


**Fig. 1.** Model of the Martian magnetic field [12]. The area studied in this work is shown on the right. The model describes the field at an altitude of 150 km.

data, allowing for improved models of the planet’s magnetic field [12–14]. Figure 1 shows [12] model of the intensity of the magnetic field of Mars at an altitude of 150 km. The MAVEN spacecraft, like MGS, is equipped with 2 fluxgate magnetometers on its solar panels. Unlike MGS, MAVEN has a non-polar elliptical orbit, with a periapsis of about 150 km (minimum altitude above the ellipsoid is 117 km).

Although many questions remain about the history and evolution of Mars’ magnetic field, it is now widely accepted that the planet once had a strong global magnetic field. This field was generated by a “dynamo” operating in the planet’s core for a sufficiently long time for minerals to acquire strong magnetization, which has persisted and provides information about Mars’ past [12].

Most of today’s hypotheses about the history and evolution of Mars’ magnetic field are based on models derived from magnetic field measurements by the MGS and MAVEN spacecraft.

The first measurements of the magnetic field on the planet’s surface were conducted by the Interior Exploration using Seismic Investigations, Geodesy and Heat Transport (InSight) mission, which successfully landed on Mars on November 26, 2018. The mission’s lander measured the surface magnetic field, which was found to be 7–10 times stronger than predicted by global models based on orbital data [15]. This difference in measurements highlights that some aspects of the magnetic field, such as local anomalies or small-scale structures, cannot be adequately captured by orbital observations.

On May 14, 2021, the lander of the Chinese mission “Tianwen-1”, carrying the rover “Zhurong”, made a soft landing on Utopia Planitia at 25°03’N, 109°55’E. In the same year, the rover traveled a distance of 1 km and measured a very weak magnetic field along its route. The measured magnetic field intensity was one-tenth of the predicted values [16]. Data on magnetic measurements from the Tianwen-1 orbiter are still limited, with only daytime data at low altitudes available in the public domain.

## 2. MAIN APPROACHES TO MODELING THE MARTIAN MAGNETIC FIELD

The Equivalent Source Dipole (ESD) method is based on the assumption that the origin of the measured magnetic field can be modeled as a sum of contributions from a large number of dipole sources, uniformly distributed below the planet’s surface.

This method has several advantages: it is less sensitive to the uneven distribution of data; allows for detailed modeling of local magnetic anomalies, which is particularly important for analyzing the magnetic field of planets with rough surfaces, such as Mars. The method enables the use of both low-orbit and high-orbit data to create a unified magnetic field model.

One of the main drawbacks of the ESD method is that it does not allow for extrapolating the field below the altitude, which, in the first order, is equal to the average distance between neighboring dipoles.

The ESD method has been applied in several studies to build global-scale models of Mars' magnetic field [3, 10, 12, 17].

In [9], the spherical harmonic method is used for modeling the Martian lithospheric magnetic field. This method is based on decomposing the magnetic field into components using spherical harmonic functions, allowing the global field to be represented as a sum of contributions from various harmonic components. A modified Huber norm was used to minimize the influence of outliers. In [14], data from both MGS and MAVEN were used to construct the model.

In [18], an innovative approach using Physics-Informed Neural Networks (PINN) is proposed, integrating physical principles into neural networks to create an improved model of the Martian crustal magnetic field. This method applies combined data from MGS and MAVEN missions, achieving high detail and increased modeling accuracy.

In this work, the method of S-approximations, described in more detail below, was applied.

### 3. S-APPROXIMATIONS

This work employs the method of linear integral representations, which allows approximating the field by summing simple and double layers (potential theory) placed on certain supports below a given topography. One variant of this method is S-approximations [19–21], which ultimately result in relatively simple analytical formulas for calculating matrix elements when solving a system of linear algebraic equations (SLAE). The S-approximations method is highly flexible and versatile, allowing not only the creation of highly accurate approximations of the magnetic field based on large volumes of satellite data but also performing various transformations, including constructing analytical continuations of the model field in two directions: from sources to observation points and from observation points to sources, enabling, in particular, the reduction of data to one altitude. Let's briefly describe the essence of S-approximations. Suppose there are  $N$  measurements ( $\geq 10^4$ ). In the first equation, we separate the useful signal from noise.

$$f_{i,\delta} = f_i + \delta f_i, \quad i = \overline{1, N} \quad (1)$$

$f_i$  is the useful signal,  $\delta f_i$  is the noise. The following relationships hold:

$$f_i = \sum_{r=1}^R \int_{M_r} \rho_r(\xi) Q_r^{(i)}(\xi) d\mu_r(\xi), \quad (2)$$

where  $\rho_r(\xi)$  are unknown functions,  $Q_r^{(i)}(\xi)$ ,  $r = \overline{1, R}$ ,  $i = \overline{1, N}$  are given functions,  $\mu_r(\xi)$  are given measures on  $M_r$ , and  $M_r$  are sets of associated points (generally in  $R^n$ ,  $n \geq 1$ ). The unknown functions  $\rho_r(\xi)$  can be interpreted as densities of simple and double layers placed on a certain surface, which can be represented by a plane, dihedral angle, or sphere. These densities can be considered as projections of magnetic sources onto supported magnetic masses, although the masses themselves have a three-dimensional structure. The main method for finding the functions  $\rho_r(\xi)$  is iterative and resembles the Newton method. During each iteration, the method of linear integral representation is modified compared to the previous step. Generally, the method for finding  $\rho_r(\xi)$  (determining the integral representations of values  $f_i$ ,  $i = \overline{1, N}$ ) involves formulating and solving a conditional variational problem. Ultimately, the problem reduces to solving a SLAE

$$A\lambda = f_\delta, \quad f_\delta = f + \delta f, \quad (3)$$

where  $\lambda$  is an  $N$ -dimensional column vector to be determined,  $A$  is a symmetric positive definite  $N \times N$  matrix with natural elements (positive on the cone), and  $f_\delta$  is an  $N$ -dimensional column vector representing the observed magnetic functional, which is expressed as the sum of the useful signal vector  $f$  and the noise vector  $\delta f$ . It is impossible to precisely and objectively isolate errors and separate  $f_\delta$  into  $f$  and  $\delta f$ .

If  $f_{i,\delta}$  represent measured values of the anomalous magnetic field, such values are considered as integral representations of the anomalous field of a quantitative type, for which the term “metrological” is used. In the same natural data, multiple metrological linear integral approximations can be found. Thus, finding a stable approximate solution to the SLAE is the key computational procedure in S-approximations.

In this work, the idealized model of Mars is represented as a sphere of radius  $R_0$ , while the actual closed surface  $S$  is considered to deviate insignificantly from this sphere, remaining within it. On the surface  $S$ , in certain points, values of a harmonic function defined in the external region of the sphere are given. This function represents the magnetic field potential, expressed through known components. These components may include, for example, the first vertical derivative of the potential on a given relief above the physical surface of Mars or one of the measured components of the magnetic induction vector.

For approximating the anomalous magnetic field, models of simple and double layers distributed over two concentric spheres located beneath the planet’s surface are used. The choice of this model is due to the relative simplicity and convenience of the matrix elements format, ensuring high computational speed.

$$\begin{aligned}
 a_{ij} = a_{ji} &= \int_0^{2\pi} \int_0^\pi \left( Q_i^{(1)}(\xi) Q_j^{(1)}(\xi) + Q_i^{(2)}(\xi) Q_j^{(2)}(\xi) \right) \sin \vartheta d\vartheta d\varphi \\
 &= \frac{2\pi}{r_i r_j \sqrt{h_i h_j}} \left( 1 + \frac{1}{4r_i r_j h_i h_j} \right) \times F \left( 2 \tan^{-1} \left( \sqrt{h_i h_j} \right), \sqrt{\frac{1 + \cos(\alpha_{ij})}{2}} \right) \\
 &\quad - \frac{\pi \left( 3h_i^2 h_j^2 - 4h_i h_j \cos(\alpha_{ij}) + 1 \right)}{r_i^2 r_j^2 h_i h_j \left( \sqrt{1 - 2h_i h_j \cos(\alpha_{ij}) + h_i^2 h_j^2} \right)^3},
 \end{aligned} \tag{4}$$

where  $F$  is the incomplete elliptic integral of the first kind [22].

Thus, the matrix  $A$  integrates both the geometry of the measurements and the information about the field sources. In this context, data processing can be interpreted as one of the stages of the regularization process. The degree of accuracy with which the field can be reconstructed using S-approximations is determined by the number of observation points, their mutual arrangement, the topography of the investigated area, and other factors.

#### 4. FEATURES OF MODELING MARS’ MAGNETIC FIELD

Data collected at various altitudes and different times using different spacecraft have varying resolution and accuracy. The uneven density of measurement data over different areas creates difficulties in constructing models.

Measurements of Mars’ magnetic field at satellite altitudes are influenced by external factors such as the interplanetary magnetic field, solar wind, coronal mass ejections, and the planet’s own magnetosphere. To minimize distortions caused by these factors, special methods of data filtering and processing are required.

Determining the sources of the magnetic field from orbital measurements represents an inverse problem with many possible solutions. To choose the most probable model among these multiple

solutions, regularization and optimization methods are used. However, these methods may impose constraints and assumptions on the final result, including limiting the possibilities of field transformations.

Constructing highly detailed models requires significant computational resources.

The topographical features of Mars also contribute to the formation of the magnetic field and must be taken into account when modeling.

## 5. DATA SELECTION

In this study, we focused on the data from the MAVEN mission. We used calibrated in-situ-calibrated level 2 data [23]. These data are presented in physical units and averaged at a uniform frequency. Up to an altitude of 500 km, data is recorded at a frequency of 1 measurement every 4 seconds, and above that, 1 measurement every 8 seconds. In addition to magnetic field measurements, the time and position of the spacecraft, the In situ dataset includes key parameters and ephemeris information obtained both from the spacecraft's instruments and from SPICE libraries, with each measurement corresponding to 235 features (columns). We used data starting from October 18, 2014, to exclude missing measurement values. The number of measurements (rows) up to and including May 15, 2024, was 38 140 693.

The MAVEN spacecraft moves in an elliptical orbit, with its altitude above the surface of Mars varying from 116 km to 6500 km (see Fig. 2). Data was collected at lower orbits, averaging less than 150 km until 2021. Measurements are available in the range from 75 degrees south latitude to 75 degrees north latitude.

The observed magnetic field values represent a superposition of the external magnetic field and the constant crustal magnetic field. In [12], an approach is proposed based on the analysis of data obtained at altitudes up to 600 km. Given that the measurement frequency in the dataset is constant up to an altitude of 500 km, and considering our interest in studying the magnetic field in close proximity to the planet, we limited the data selection to an altitude of 500 km. Figure 3 illustrates the dependence of the measured values of the magnetic field components  $B_x$ ,  $B_y$ ,  $B_z$  on the altitude above the surface of Mars. There is a general trend of decreasing magnetic field strength with increasing altitude. However, the presence of the external magnetic field, namely the interplanetary magnetic field associated with the solar wind, is also observed. This external influence manifests as deviations from the monotonic decrease in the magnetic field. This observation highlights the complexity of the magnetic environment near Mars and the need to account for various sources when interpreting magnetic field measurements (see [24–26]).

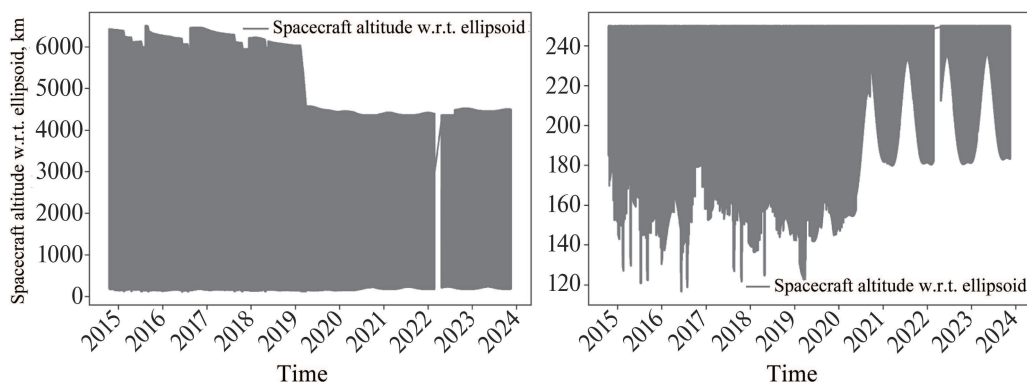


**Fig. 2.** Altitude profiles of measurements obtained by MAVEN from 2014 to 2024. A fragment of data limited to an altitude of 250 km is shown on the right.

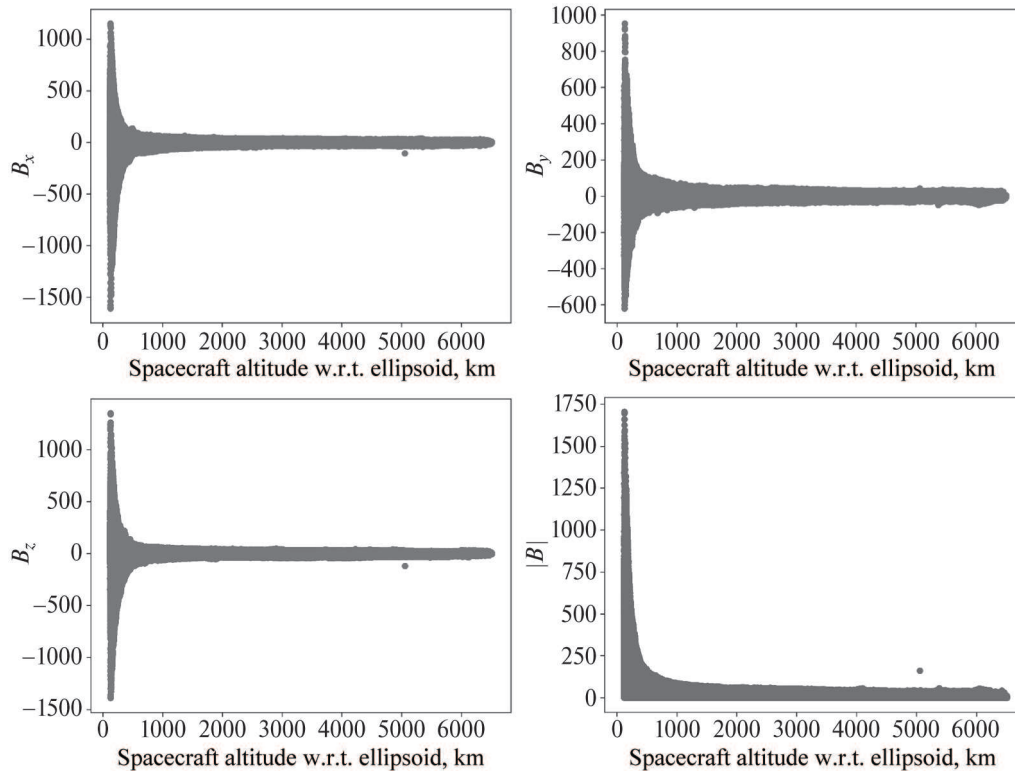


**Fig. 3.** Altitude profile of magnetic field components. The scatter plot illustrates the decrease in the values of the magnetic field components  $B_x$ ,  $B_y$ ,  $B_z$  with increasing altitude.

Data samples were made both on a rectangular grid with a step of 0.5 degrees and on an equal-area SREAG grid [27]. In the following examples, the results for the sample on the rectangular grid are presented.

For constructing the analytical approximation and analytical continuation of the field, the following region was chosen: from  $25^\circ$  S to  $35^\circ$  N, from  $100^\circ$  E to  $160^\circ$  E. This area includes the landing site of the InSight mission spacecraft in the Elysium Plain,  $4.502^\circ$  N,  $135.623^\circ$  E ([28]), as well as the landing site of the Zhurong rover on the Utopia Plain,  $25.066^\circ$  N,  $109.926^\circ$  E [29].

The minimum altitude at which measurements were taken over the studied region is 119.4 km. Limiting the sample to nighttime data significantly affects the overall picture and greatly reduces the range of observed values. In particular, the minimum measurement altitude at some points exceeds 450 km.

Each measurement was matched to a grid node if the deviation of its latitude and longitude from the corresponding coordinates of the node did not exceed  $0.25^\circ$ . The original coordinates of the measurements were used for constructing the approximation. In this work, samples of magnetic field measurement data obtained at minimum altitudes above the grid nodes were analyzed.

As seen in Fig. 4, which presents an example of measurements of the  $B_z$  component, nighttime data shows significantly lower noise levels compared to daytime data, as they are less affected by external magnetic disturbances, providing a higher signal-to-noise ratio. This makes nighttime data preferable for modeling the lithospheric magnetic field, ensuring more accurate and reliable results.

Daytime data, on the other hand, can be significantly distorted by solar activity such as solar flares. Additional contributions are made by currents generated in the Martian ionosphere under the influence of solar radiation. By limiting the sample to nighttime data, we minimize the influence of these factors.

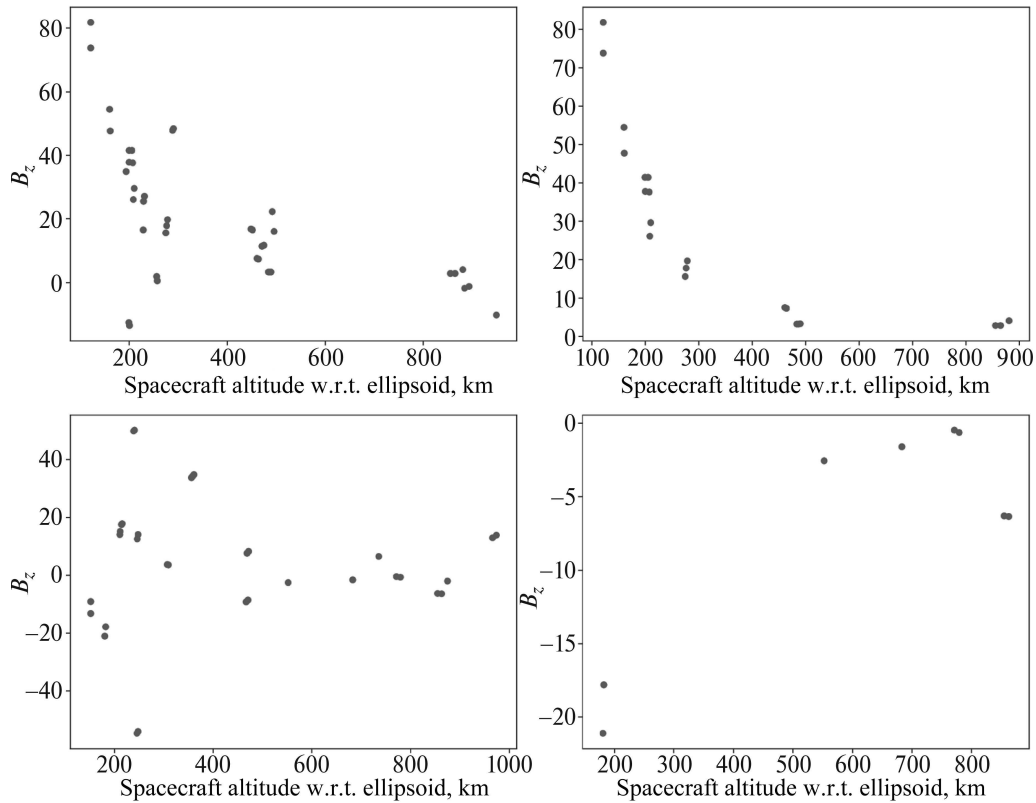


**Fig. 4.** Top—measurements of the vertical magnetic field component ( $B_z$ ) over a point with coordinates  $0^\circ$  N,  $0^\circ$  E ( $\pm 0.5^\circ$ ) up to an altitude of 1000 km. Bottom—similar measurements taken over the InSight mission landing site.

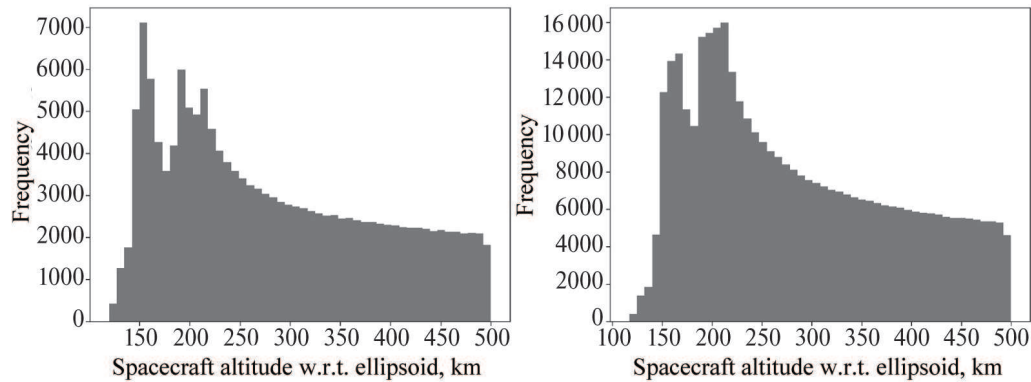


**Fig. 5.** Frequency distribution of observation altitudes over the selected study area. Left—for nighttime data, right—all data.

Following the recommendations given in [12], we define nighttime data as measurements obtained from 19:00 to 5:00 local spacecraft time. In [15], dedicated to the analysis of the magnetic field at the InSight mission landing site, the authors use a narrower time interval—from 20:00 to 4:00—for even stricter minimization of the contribution of external fields. However, using a narrower time window significantly reduces the volume of available data, negatively affecting the statistical significance and representativeness of the sample. Overall, strict time selection can lead to the exclusion of important measurements at low altitudes, crucial for more accurate modeling of the lithospheric magnetic field.

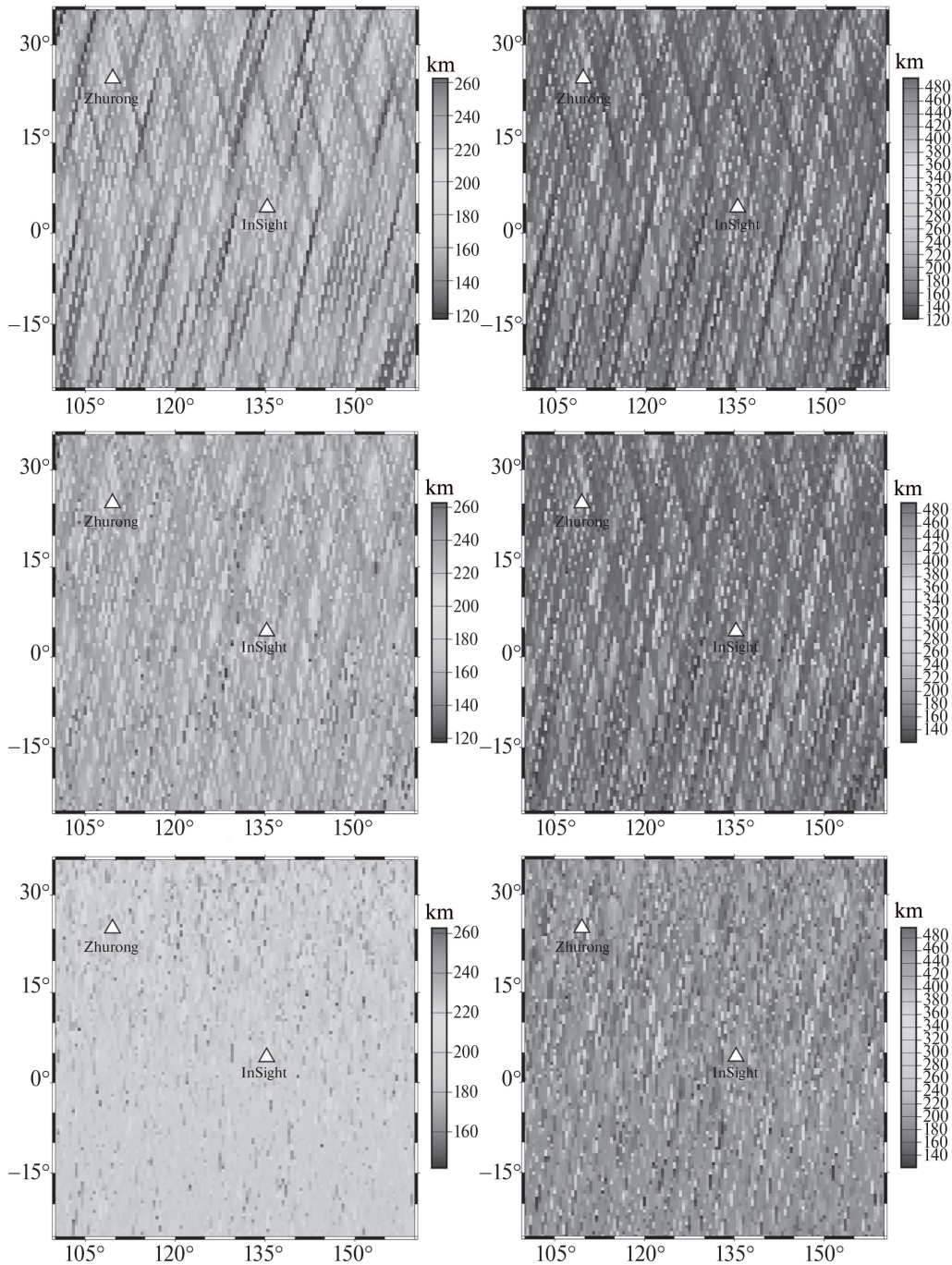


**Fig. 6.** Maps of measurement altitudes for various data samples.

In our work, priority is given to data collected at low altitudes, as they play a key role in creating high-resolution and accurate models of the Martian lithospheric magnetic field. Measurements at low altitudes are taken closer to the sources of the magnetic field, allowing for a more detailed identification and characterization of small-scale magnetic anomalies and structural features of the field.

When forming the sample using both nighttime and daytime data, at least one measurement at an altitude up to 500 km was found for each grid node. When limiting the sample to nighttime data only, the share of nodes without attached values was 0.2.



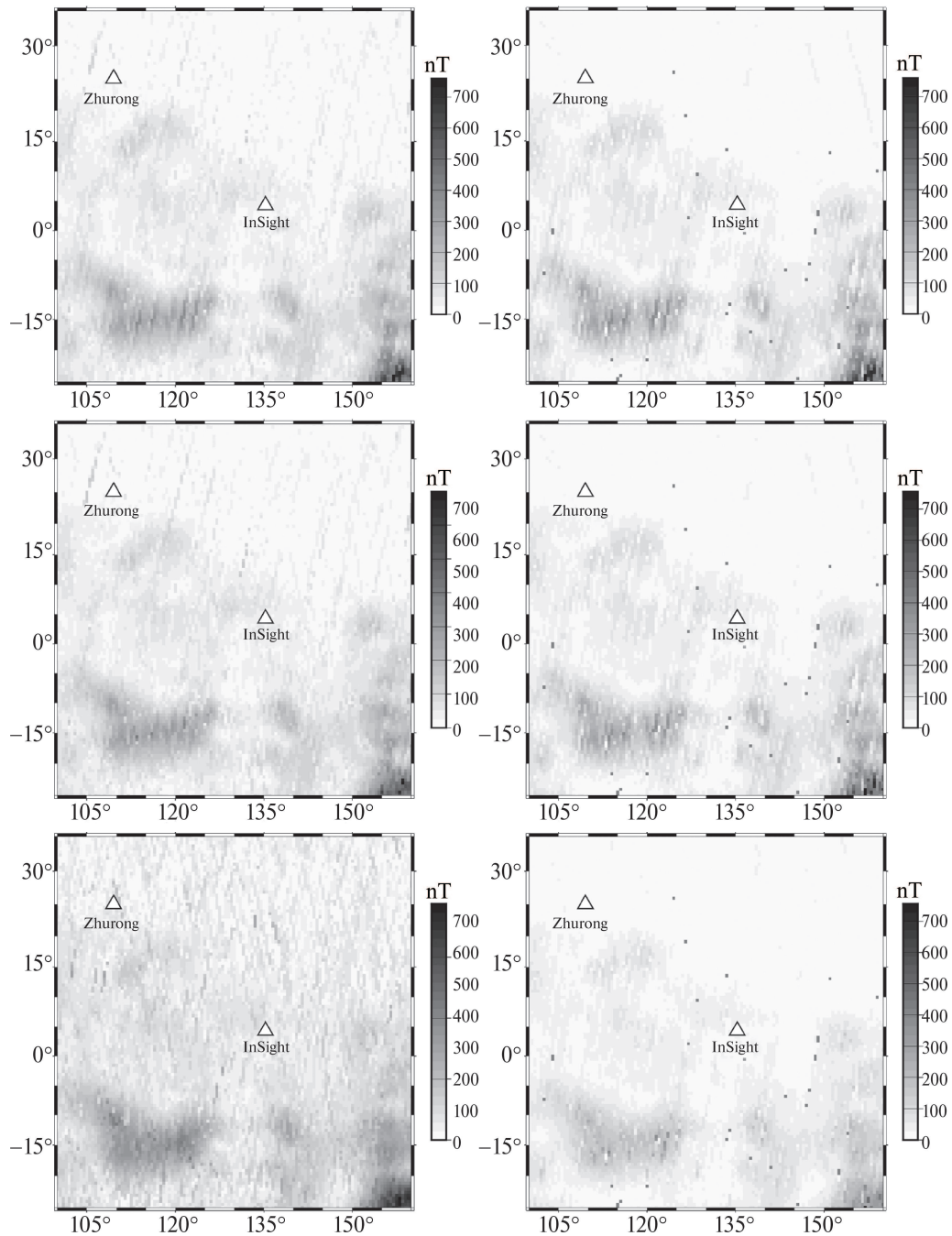


**Fig. 7.** Magnetic field intensity depending on the chosen measurement altitude criterion.

From the histogram in Fig. 5, it can be seen that due to the elliptical orbit of the MAVEN spacecraft, the highest frequency of measurements in the studied area is concentrated at altitudes close to the planet's surface. Two characteristic peaks of the distribution are clearly distinguished—around 150 km and 190 km.

When solving the inverse problem using the S-approximation algorithm, the optimal choice is the measurement data obtained at the closest altitudes. Taking this requirement into account, three different data samples were formed: at the minimum recorded altitudes; at altitudes closest to the mode of the altitude distribution above the grid nodes ( $\sim 150$  km); at altitudes corresponding to the second peak of measurement frequency observed in the histogram ( $\sim 190$  km). Figure 6

illustrates the spatial distribution of altitudes for each of these samples. Top—distribution of minimum altitudes, middle—distribution of altitudes closest to the 150 km distribution mode, bottom—distribution of altitudes closest to the second peak of the measurement frequency 190 km. Left—using both night and day data, right—using only night data. This representation allows assessing the vertical structure of the measurements and its variations depending on the chosen data selection criterion. Figure 7 demonstrates the the values of the measured magnetic field strength at the altitudes corresponding to the samples presented in Fig. 6, taking into account various selection criteria by altitude. This allows visualizing the spatial variations of the magnetic field and assessing the impact of measurement altitude on the recorded values. This approach to forming samples provides the possibility of comparative analysis of the magnetic field at different altitude levels, which is important for the correct interpretation of the data.

## 6. RESULTS OF APPROXIMATION

The key parameters defining the model of the anomalous magnetic field obtained using the S-approximation method were the radii of the anomaly. Experiments were conducted with varying depths of spheres beneath the surface of an idealized spherical planet with a radius of 3393.5 km, ranging from 0.1 km to 50.0 km. The results of the experiments demonstrate the high accuracy of the anomalous magnetic field approximation using the S-approximation method. table provides the approximation results for different samples obtained when the sources of the magnetic field were located at depths of 20 and 40 km. In the experiments labeled “DN”, both nighttime and daytime data were used, while “N” used only nighttime data. Everywhere, the quality index of the solution  $\Delta = \frac{\|A\lambda - f_\delta\|}{\|f_\delta\|} < 10^{-8}$ , and the root-mean-square deviation  $\sigma_0 = RMSE = \frac{\|A\lambda - f_\delta\|}{\sqrt{N}} < 10^{-8}$ ,  $\sigma_{\min} = \min |A\lambda - f_\delta|$ ,  $\sigma_{\max} = \max |A\lambda - f_\delta|$ . Here  $\|f_\delta\|$  is the Euclidean norm,  $N$  is the number of points,  $\sigma_{\min}$  is the minimum absolute value of the error, and  $\sigma_{\max}$  is the maximum absolute value of the error. The root-mean-square deviations of the data from the analytical approximation for the samples presented in table are shown in Fig. 8. Top—distribution of minimum altitudes, middle—distribution of altitudes closest to the 150 km distribution mode, bottom—distribution of altitudes closest to the second peak of the measurement frequency 190 km. Left—using both night and day data, right—using only night data.

Bringing the magnetic field to a unified altitude using the S-approximation method is a complex but important task. In this work, an analytical continuation of the components of the measured magnetic field at altitudes close to the mode of the 150 km distribution was performed to a unified altitude of 150 km. The results of the point-by-point analytical continuation of the field to the unified altitude of 150 km are presented in Fig. 9, where a comparison with the model proposed in [12] is also provided. On the left—initial measurements of  $B_r$  at altitudes closest to 150 km, in the center—analytical continuation of the  $B_r$  field to a single altitude of 150 km using the regional S-approximation method, on the right—difference between the initial data and the result of the continuation.

Approximation results for various data samples

Experiment	Number of points $N$	$\sigma_0$	$\sigma_{\min}$	$\sigma_{\max}$	$\Delta$
DN-min	14641	8.371e-09	1.662e-12	3.211e-08	1.858e-10
DN-150	14641	8.283e-09	6.341e-13	3.489e-08	1.935e-10
DN-190	14641	8.519e-09	1.570e-12	3.480e-08	2.484e-10
N-min	14610	3.902e-09	4.423e-13	1.756e-08	9.839e-11
N-150	14610	4.259e-09	1.065e-13	1.730e-08	1.117e-10
N-190	14610	3.149e-09	1.900e-13	1.423e-08	1.067e-10

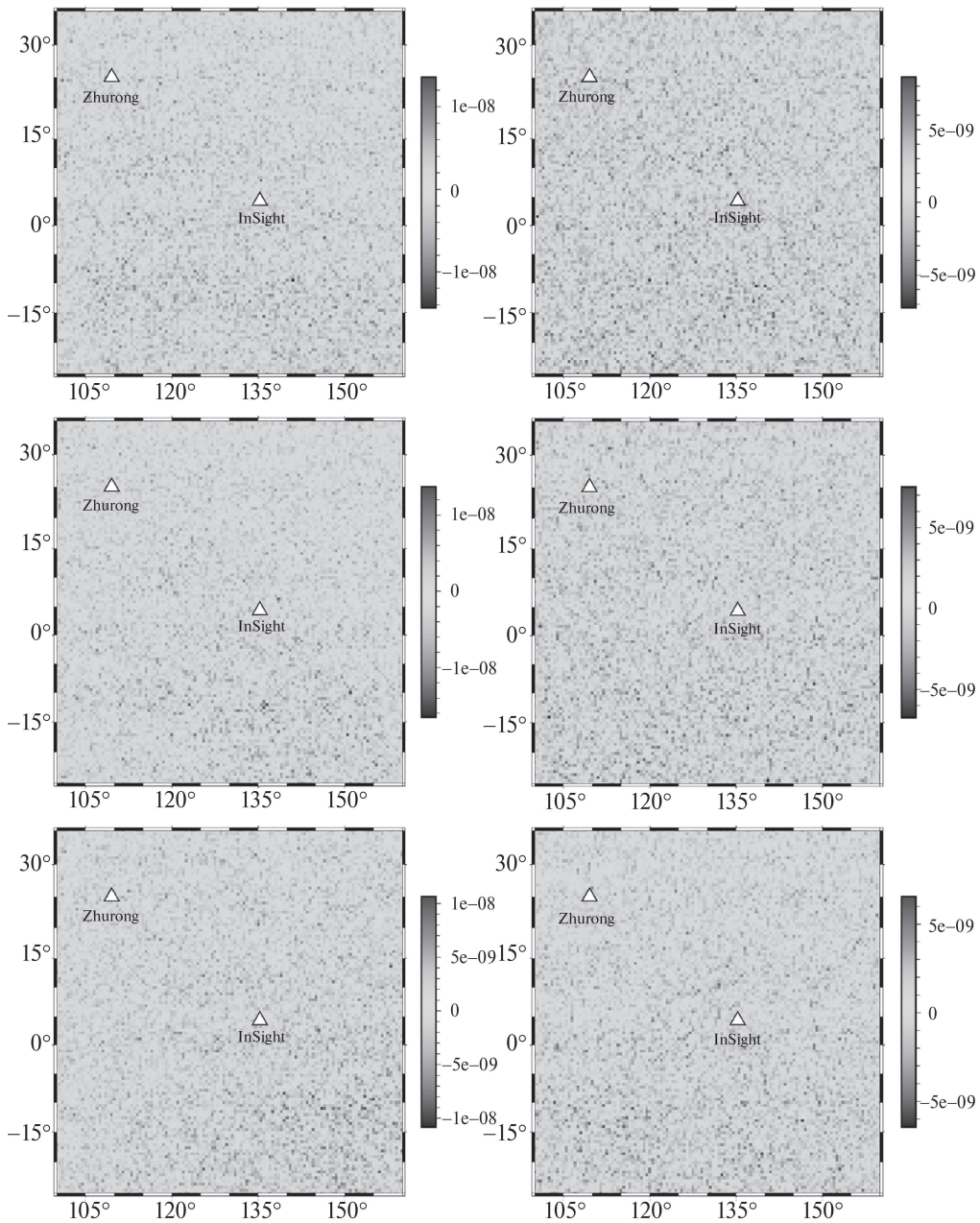


**Fig. 8.** Root-mean-square deviations of the data from the analytical approximation for the samples presented in table.

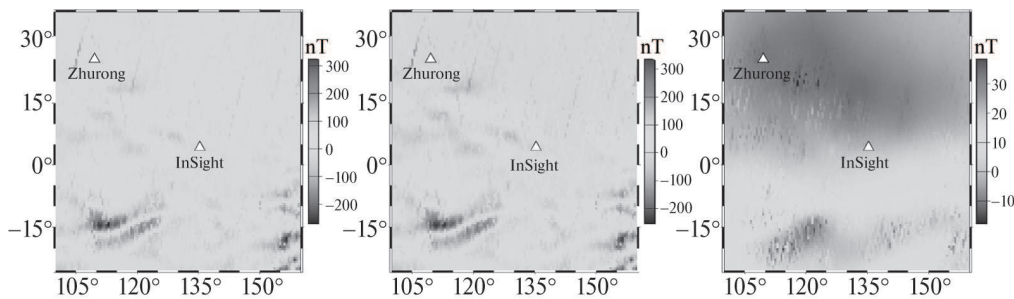


**Fig. 9.** Comparison of original data and the result of analytical continuation.

## 7. CONCLUSION

In this study, detailed processing and analysis of magnetic field measurement data from Mars, obtained by the MAVEN spacecraft, were conducted. Various data samples were formed, including nighttime and daytime measurements at different altitudes. The conducted research demonstrates the importance of a careful approach to the selection and preliminary processing of satellite measurement data when modeling the planet's magnetic field. Restricting the sample to nighttime data significantly improves the signal-to-noise ratio, which is especially important for studying weak magnetic anomalies. However, this leads to a reduction in the total amount of available data, which can be a limiting factor when constructing global magnetic field models. The obtained results highlight the importance of a meticulous approach to forming data samples when constructing global magnetic field models of the planet. Considering the spacecraft's orbit characteristics, temporal variations of the magnetic field, and characteristic measurement altitudes allows for improving the quality and reliability of the obtained models.

The results demonstrate that the S-approximation method is an effective tool for modeling the Martian magnetic field. The root-mean-square deviations of the model from the measurements are less than  $10^{-8}$  nT, indicating a high accuracy of anomalous magnetic field approximation with various model parameters and data sample criteria. The analytical continuation of the magnetic field to a unified altitude allows for obtaining a consistent regional field model comparable to existing global models. An important aspect is the chosen depth of the magnetic field sources. In this study, depths of 20 and 40 km were considered, corresponding to the assumptions about the location of magnetic anomalies in the Martian lithosphere. The calculation results also showed that the S-approximation method adequately models the field at various source depths.

Further research can be aimed at developing optimal strategies for combining data from different samples, expanding the modeling area, and creating a detailed global magnetic field model of Mars, as well as integrating measurement data from the MGS and MAVEN missions to enhance the spatial and temporal coverage of measurements. It is necessary to separately compare the analytical continuations of the magnetic field obtained by the S-approximation method to the planet's surface with ground measurements and geological structure data. Combining data samples obtained by different criteria can provide a more complete understanding of the structure and variations of the magnetic field on various scales.

## FUNDING

This work was supported by the Russian Science Foundation, project no. 23-27-00392 (<https://rscf.ru/project/23-27-00392/>).

## REFERENCES

1. Acuña, M.H., Space-based magnetometers, *Rev. Scientific Instrum.*, 2002, vol. 73, no. 11, pp. 3717–3736.
2. Breus, T.K., Verigin, M.I., Kotova, G.A., et al., Characteristics of the Martian Magnetosphere according to the Data of the Mars 3 and Phobos 2 Satellites: Comparison with MGS and MAVEN Results, *Cosmic Res.*, 2021, vol. 59, no. 6, pp. 478–492.
3. Langlais, B., Purucker, M.E., and Manda, M., Crustal magnetic field of Mars, *J. Geophys. Res.*, 2004, vol. 109, no. E02008.
4. Acuña, M.H., The magnetic field of Mars, *Leading Edge*, 2003, vol. 22, no. 8, pp. 769–771.
5. Arkani-Hamed, J., Magnetization of Martian lower crust: Revisited, *J. Geophys. Res.*, 2007, vol. 112, no. E5, 2006JE002824.
6. Cain, J.C., Ferguson, B.B., and Mozzoni, D., An  $n = 90$  internal potential function of the Martian crustal magnetic field, *J. Geophys. Res.*, 2003, vol. 108, no. E2, 5008.
7. Chiao, L., Lin, J., and Gung, Y., Crustal magnetization equivalent source model of Mars constructed from a hierarchical multiresolution inversion of the Mars Global Surveyor data, *J. Geophys. Res.*, 2006, vol. 111, no. E12010.

8. Lillis, R.J., Frey, H.V., and Manga, M., Rapid decrease in Martian crustal magnetization in the Noachian era: Implications for the dynamo and climate of early Mars, *Geop. Res. Lett. John Wiley & Sons, Ltd*, 2008, vol. 35, no. L14203.
9. Morschhauser, A., Lesur, V., and Grott, M., A spherical harmonic model of the lithospheric magnetic field of Mars, *J. Geophys. Res.: Planets*, John Wiley & Sons, Ltd, 2014, vol. 119, no. 6, pp. 1162–1188.
10. Purucker, M., Ravat, D., Frey, H., et al., An altitude-normalized magnetic map of Mars and its interpretation, *Geop. Res. Lett.*, 2000, vol. 27, no. 16, pp. 2449–2452.
11. Whaler, K.A. and Purucker, M.E., A spatially continuous magnetization model for Mars, *J. Geophys. Res.: Planets*, John Wiley & Sons, Ltd, 2005, vol. 110, no. E9.
12. Langlais, B., Thébault, E., Houliez, A., et al., A New Model of the Crustal Magnetic Field of Mars Using MGS and MAVEN, *JGR Planets*, 2019, vol. 124, no. 6, pp. 1542–1569.
13. Mittelholz, A., Johnson, C.L., and Morschhauser, A.A., A New Magnetic Field Activity Proxy for Mars From MAVEN Data, *Geop. Res. Lett.*, 2018, vol. 45, no. 12, pp. 5899–5907.
14. Gao, J.W., Rong, Z.J., Klinger, L., et al., A Spherical Harmonic Martian Crustal Magnetic Field Model Combining Data Sets of MAVEN and MGS, *Earth Space Science*, 2021, vol. 8, no. 10, e2021EA001860.
15. Johnson, C.L., Mittelholz, A., Langlais, B., et al., Crustal and time-varying magnetic fields at the InSight landing site on Mars, *Nature Geoscience*, 2020, vol. 13, no. 3, pp. 199–204.
16. Du, A., Ge, Y., Wang, H., et al., Ground magnetic survey on Mars from the Zhurong rover, *Nature Astronomy*, 2023, vol. 7, no. 9, pp. 1037–1047.
17. Langlais, B., Lesur, V., Purucker, M.E., et al., Crustal Magnetic Fields of Terrestrial Planets, *Space Sci Rev.*, 2010, vol. 152, no. 1–4, pp. 223–249.
18. Delcourt, T. and Mittelholz, A., A new model of the lithospheric magnetic field of Mars using a physics-informed neural network, *Tenth International Conference on Mars 2024* (LPI Contrib. no. 3007).
19. Strakhov, V.N. and Stepanova, I.E., Solution of gravity problems by the S-approximation method (regional version), *Izvestiya. Physics of the Solid Earth*, 2002, vol. 38, no. 7, pp. 535–544.
20. Stepanova, I.E., On the S-approximation of the Earth’s gravity field: regional version, *Inverse Problems in Science and Engineering*, 2009, vol. 17, no. 8, pp. 1095–1111.
21. Stepanova, I.E., Salnikov, A.M., Gudkova, T.V., et al., On finding the analytical continuation of the magnetic field of Mars from satellite data using a combined approach, *Geop. Res.*, 2023, vol. 24, no. 2, pp. 58–83.
22. Carlson, B.C., Computing elliptic integrals by duplication, *Numer. Math.*, 1979, vol. 33, no. 1, pp. 1–16.
23. The Planetary Plasma Interactions (PPI) Node of the Planetary Data System (PDS) <https://search-pdspipi.igpp.ucla.edu>.
24. Langlais, B., Civet, F., and Thébault, E., In situ and remote characterization of the external field temporal variations at Mars, *J. Geophys. Res.: Planets*, John Wiley & Sons, Ltd, 2017, vol. 122, no. 1, pp. 110–123.
25. Mittelholz, A., Johnson, C.L., and Lillis, R.J., Global-scale external magnetic fields at Mars measured at satellite altitude, *J. Geophys. Res.: Planets*, 2017, vol. 122, no. 6, pp. 1243–1257.
26. Mittelholz, A., Johnson, C.L., Fillingim, M., et al., Mars’ External Magnetic Field as Seen From the Surface With InSight, *J. Geophys. Res.: Planets*, John Wiley & Sons, Ltd, 2023, vol. 128, no. 1, e2022JE007616.
27. Malkin, Z., A New Equal-area Isolatitudinal Grid on a Spherical Surface, *AJ*, 2019, vol. 158, no. 4, p. 158.
28. Du, A., Ge, Y., Wang, H., et al., 1. Golombek M., Kass D., Williams N., et al. Assessment of InSight Landing Site Predictions, *J. Geophys. Res.: Planets*, John Wiley & Sons, Ltd, 2020, vol. 125, no. 8, e2020JE006502.
29. “Tianwen-1 Lander and Zhurong Rover in Southern Utopia Planitia (ESP\_069665\_2055)”. [https://hirise.lpl.arizona.edu/ESP\\_069665\\_2055](https://hirise.lpl.arizona.edu/ESP_069665_2055)

*This paper was recommended for publication by A.A. Galyaev, a member of the Editorial Board*